JOURNAL OF GEOPHYSICAL RESEARCH, VOL. 95, NO. B6, PAGES 8647–8661, JUNE 10, 1990

The Solid-State Flow of Polymineralic Rocks

MARK R. HANDY

Geologisches Institut, Universität Bern, Bern, Switzerland

Polymineralic rocks display three end-member types of mechanical and microstructural behavior: (1) strong minerals form a load-bearing framework that contains spaces filled with weaker minerals; (2) two or more minerals with low relative strengths control bulk rheology and form elongate boudins; (3) one very weak mineral governs bulk rheology, while the stronger minerals form clasts. A concept of strain energy partitioning in polyphase aggregates allows the expression of the bulk strength of a rock in terms of its strain rate, temperature, and the volume proportions and rheological properties of its constituent minerals. Bimineralic strength versus composition relations predicted with this model are highly nonlinear and mimic the rheological behavior of experimentally deformed bimineralic aggregates. Quantitative analysis of microstructures in quartzo-feldspathic tectonites suggests that foliation development leads to a significant reduction in rock strength. This is due to decreased stress concentration within the deforming aggregate as matrix and clast grain size is reduced and the average spacing between strong minerals increases.

1. INTRODUCTION

The solid-state flow of rocks is commonly simulated by extrapolating steady state laboratory flow laws for monomineralic aggregates to natural strain rates and temperatures in the lithosphere [e.g., *Carter*, 1976; *Brace and Kohlstedt*, 1980; *Kirby*, 1980; *Carter and Tsenn*, 1987]. This approach is valid if one mineral is sufficiently weak or abundant with respect to the other minerals to actually control the rheology of the rock and if the microstructure and rheology of the rocks do not vary greatly with strain. However, microstructural studies of polymineralic tectonites usually show that several minerals (rather than just one very weak mineral) are deformed and collectively determine the rheology of the aggregate [e.g., *White et al.*, 1980]. Ductile and brittle faulting involve drastic localized changes in microstructure (e.g., grain size reduction, foliation development) which effect changes in the dominant deformation mechanisms governing the flow of polymineralic rocks [e.g., *White*, 1976]. The extrapolation of laboratory flow laws for polymineralic rocks to natural strain rates is problematic because the constituent minerals have differing nonlinear creep strengths [*Kronenberg and Shelton*, 1980; *Horowitz et al.*, 1981]. In nature, both stress and strain are partitioned according to the relative creep characteristics of the minerals making up the rocks. As will be shown in this paper, the degree of stress and strain partitioning in a deforming rock depends strongly on the proportions, shape, and distribution of the minerals, as well as on the temperature, strain rate, and grain size dependencies of creep in these phases. The effect of strain on such rock-specific characteristics bears important implications for long-term lithospheric rheology.

2. REVIEW OF PREVIOUS WORK

Experimental deformation of two solid-phase aggregates indicates that the weakest phase exerts a disproportionately large effect on the strength of the aggregate [*Le Hazif*, 1978]. Strength versus composition relations in rocks are highly nonlinear, such that the weakest mineral governs the strength of the rock for volume proportions of the weak mineral, ϕ_w, ranging from about 0.3 to 1.0 [*Shelton and Tullis*, 1981; *Price*, 1982; *Jordan*, 1987; *Ross et al.*, 1987]. *Carter et al.* [1981] showed that the activation energy of creep of dry Westerly Granite is closest to that of quartz, the mineral which was microscopically observed to have accommodated the most strain. For rocks with very low volume proportions of the weakest mineral ($\phi_w < 0.3$), *Tharp* [1983] has drawn an analogy between the weakening effect of pores on the strength of powder metals and the weakening effect of a sufficiently weak mineral on the strength of a polymineralic rock. Provided that the strong phase forms a load-bearing framework and the relative strength of the constituent phases is 10 or more, the bulk strength of a deforming aggregate depends primarily on the strength of the strong phase and on the shape and distribution of the space that contains the weak phase [*Eudier*, 1962; *Ishimaru et al.*, 1971; *Griffith et al.*, 1979]. *Jordan* [1988] described the deformational behavior of bimineralic rocks as a combination of the Eudier-Tharp model for low ϕ_w and a planar "two-block" model for intermediate to high ϕ_w compositions. In the planar two-block model, the weak mineral forms an interconnected matrix, and the strong mineral is assumed to be rheologically passive. Jordan's concept is very similar to that proposed by *Arzi* [1978] for the rheology of partially melted rocks and demonstrated experimentally for partially molten granite [*Van der Molen and Paterson*, 1979]. Recent experiments on partial melt rheology also demonstrate the nonlinear dependence of strength on suspension density and melt composition [*Ryerson et al.*, 1988].

To a first approximation, polymineralic rocks undergoing subsolidus, solid-state flow can be compared to a suspension of rigid spheres in a viscous liquid. *Einstein*'s [1906, 1911] classical treatment of suspensions adequately predicts the rheology of dilute suspensions but breaks down at high suspension concentrations. Subsequent attempts to extend Einstein's hydrodynamic theory to dense suspensions [e.g., *Roscoe*, 1952; *Frankel and Acrivos*, 1967] are limited by the assumption of an idealized, invariant packing configuration of the rigid spheres. More recent investigations reveal that most inhomogeneous materials are highly thixotropic [e.g., *Gadala-Maria and Acrivos*, 1980; *Pätzold*, 1980] and that the

Paper number 90JB00243.
0148-0227/90/90JB-00243$05.00

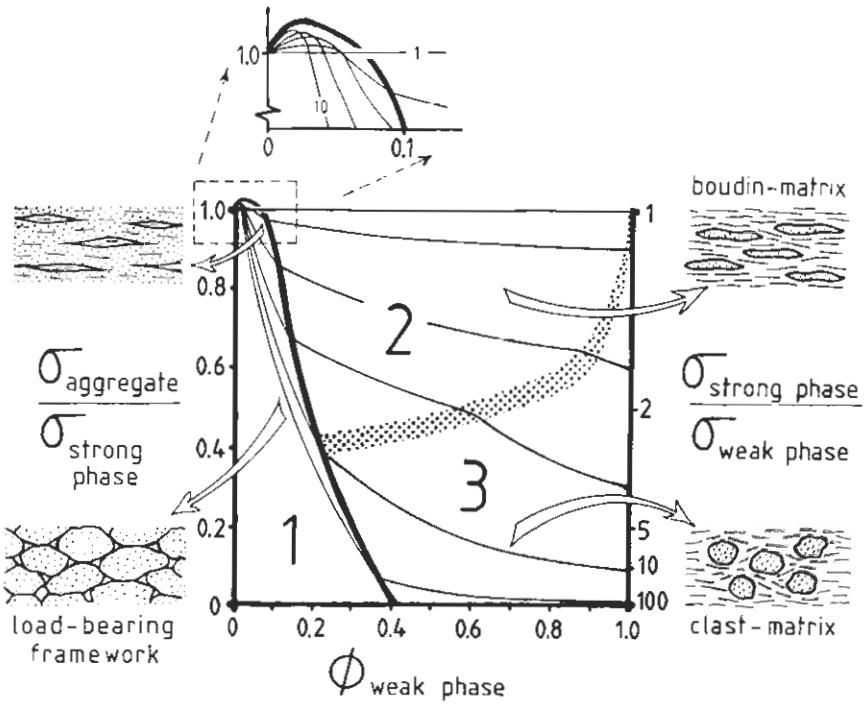

Fig. 1. Hypothetical diagram of normalized aggregate strength (left-hand axis) versus volume proportion of the weak phase (horizontal axis) for a two-phase aggregate. Right-hand axis is the relative strength of the strong and weak phases. Heavy line is the boundary between framework-supported rheologies (domain 1) and matrix-controlled rheologies (domains 2 and 3). Stippled curve indicates the transition from a boudin-matrix rheology (domain 2) to a clast-matrix rheology (domain 3). The characteristic microstructure in each of the rheological fields is depicted beside the diagram. Thin curves are the contours of normalized rock strength at various mineral strength ratios that are indicated on the right-hand axis. Expanded diagram of area in dashed box (top left) shows in detail the contours of normalized rock strength at very low volume proportions ($\phi_w < 0.1$) of weak phase.

rigid spheres in the deforming suspension tend to cluster at high strains [e.g., *Bouillot et al.*, 1982; *Brady and Bossis*, 1985].

Modelling of the slow deformation of viscous composites has so far been restricted to the special case of linear viscous materials containing ellipsoidal inhomogeneities of different viscosity [*Gay*, 1968; *Bilby et al.*, 1975]. The geological use of such models is limited by the fact that the viscous creep of most rock-forming minerals is highly nonlinear over a broad range of homologous temperatures and strain rates [e.g., *Carter*, 1976; *Schmid*, 1982]. "Self-consistent" modelling of two-phase aggregates [e.g., *Hill*, 1965; *Chen and Argon*, 1978] successfully predicts the disproportionately large rheological effect of the weakest phase but averages the effects of local stress concentration on the deforming matrix. This leads to an overestimation of deformational resistance and creep moduli of the composite [*Chen and Argon*, 1978]. The "bounding theorems" approach [*Hutchinson*, 1976] is not effective for cases where the elastic moduli of the constituent phases in the aggregate diverge (e.g., aggregates with rigid inclusions or two power law hardening materials).

Many of the experiments cited above were conducted at low coaxial strains (<40%) and at conditions favoring high strength contrasts (>10) among the phases in the aggregate. However, the complete range of rheological behavior in polyphase aggregates also includes conditions for which the strength contrasts between constituent phases are small. Such rheologies are geologically relevant, because differences in the temperature, strain rate, and grain size dependencies of creep in minerals are such that mineral strength contrasts can easily decrease to less than an order of magnitude under some natural conditions (e.g., extrapolated creep laws of *Carter and Tsenn* [1987]).

3. A Conceptual Model of Polyphase Rheology

3.1. *Microstructural Observations and Mechanical Inferences*

Polyphase aggregates show three end-member types of microstructural and mechanical behavior (Figure 1). This subdivision is based on mechanical inferences from microstructures of natural tectonites (examples in Figures 2, 3, and 5) and from experimental and theoretical work on polyphase aggregates. The compositional dependence of polyphase rheology is conveniently depicted in normalized strength versus volume-proportion diagrams such as Figure 1 [*Jordan*, 1987]. Normalized strength, $\sigma_{normalized}$, is defined as the ratio of the strength of the two-phase aggregate to the strength of the strongest phase at the temperature and strain rate of deformation. The strength ratio of the strong and weak phases ($\sigma_{strong}/\sigma_{weak}$) in the rock is shown on the right-hand axis of Figure 1. The fields are contoured for normalized rock strength at various strength ratios of the constituent phases.

Domain 1 in Figure 1 is the framework-supported field, in which the strong phase forms an interconnective, load-bearing framework that separates spaces filled with a weak

phase (example in Figure 2*a* [*Arzi*, 1978; *Tharp*, 1983]). As noted in section 2, the strength of the aggregate depends primarily on the strength of the strong phase and on the shape, size, and distribution of the weak phase. Domain 2, the boudin field, is characterized by elongate boudins of the stronger phase in a weaker matrix (Figure 3). The relative strength of the minerals is low and the significant strain in both phases indicates that both phases are rheologically active. Domain 3 is the clast-matrix field. The strong phase forms relatively undeformed clasts (Figures 2*b*, 2*c*, and 6*a*) and so is inferred to be rheologically passive. Such microstructures are indicative of higher mineral strength ratios than in domain 2.

The structural and rheological behavior outlined above reflects the stress and strain rate partitioning amongst the constituent minerals of a rock deforming at given bulk strain rate and temperature-pressure conditions. The contours of normalized rock strength at constant mineral strength ratio (thin curves in Figure 1) are generally drawn with a negative sloping, concave-upward shape since the increase in bulk strength with decreasing ϕ_w is more pronounced at high relative strengths and low volume proportions of the weak mineral. This is because strain compatibility problems arise when there is a smaller volume of rheologically active mineral present to accommodate strain or when the ductility of the stronger mineral decreases with respect to that of the weaker mineral. Both conditions induce stress concentrations in the matrix which increase the bulk strength of the aggregate (see section 4.1).

The mechanical boundary of domain 1 with domains 2 and 3 is predicted to be sharp (heavy line in Figure 1), since the geometrical transition from a framework-supported to a matrix-supported structure is discontinuous [*Arzi*, 1978]. In contrast, the boundary separating domains 2 and 3 (stippled curve in Figure 1) is probably diffuse and is marked by a slight steepening of the mineral strength ratio contours going from domain 2 to domain 3. This boundary corresponds with the onset of significant ductility in the stronger mineral, so its width depends strongly on the relative elastic properties of the minerals, as well as on the shape and spatial distribution of these minerals in the aggregate. The shape of the boundary between domains 2 and 3 is experimentally unconstrained in the absence of mechanical data for aggregates with low relative mineral strengths. However, domain 3 behavior is expected to extend to low mineral strength contrasts at very high ϕ_w (Figure 1), since stress concentrations are negligible in nearly pure, homogeneous substances. With decreasing ϕ_w, yielding of the strong mineral probably occurs at progressively higher mineral strength contrasts due to the increase in stress concentration as local strain compatibility becomes more difficult to maintain. Together, these considerations suggest a positively sloping, concave-upward shape for the diffuse boundary area separating domains 2 and 3 (Figure 1). The change in slope of the bulk strength curves across this domain boundary reflects differences between domains 2 and 3 in strain accommodation and strain compatibility within the deforming aggregate. In domain 3, only the weak mineral deforms whereas the strong mineral(s) remains rheologically passive and concentrates stress and strain in the weak matrix. In domain 2, both the strong and weak phases accommodate strain (Figure 3), so that strain compatibility requirements are relaxed and the compositional effects are less pronounced than in domain 3.

The relative strength of the constituent mineral phases in domains 2 and 3 is crudely constrained for intermediate ϕ_w values from a combination of experimental and theoretical studies. *Jordan* [1987] reports that calcite forms porphyroclasts in a matrix of halite under experimental conditions for which the creep strength of calcite is at least 10 times that of halite. Furthermore, computer simulation of deformed viscous materials indicates that a mineral strength contrast of at least 10 : 1 is necessary for porphyroclasts of a harder phase to retain their shape after large strains [*Scott*, 1987]. Taken together, these observations suggest a minimum strength contrast amongst minerals of 10 : 1 in domain 3 over intermediate to high ϕ_w values. By the same criteria, mineral strength contrasts in domain 2 are inferred to be less and probably do not exceed the 10 : 1 value for the same compositional range.

3.2. *Effects of Strain, Strain Rate, Temperature, and Pore Pressure*

The microstructural sequence in Figure 2 shows that progressive strain of a quartz diorite ($\phi_w = 0.2 - 0.3$) leads to the disintegration of the feldspar framework and to the development of a foliation which is generally parallel to the shear zone boundary (i.e., the shearing plane). Whereas the weak quartz phase initially occupies unconnected pockets in Figure 2*a*, the quartz in Figures 2*b* and 2*c* forms interconnected, microscale shear zones comprising lenticular strands of fine, dynamically recrystallized aggregates. This signifies a strain-induced transition from a framework-supported to a matrix-supported rheology and is observed in experiments to coincide with a significant decrease in rock strength [*Le Hazif*, 1978; *Jordan*, 1987]. Thus, prior to straining or at very low strains, the boundary curve for domain 1 is inferred to form a broad shoulder at ϕ_w of 0 to ~0.30 (thick dashed line in Figure 4*a*). Progressive straining and "foliation weakening" [*Jordan*, 1987] results in a downward movement of most of the boundary curve to lower normalized strengths (arrow and thick solid line in Figure 4*a*). In experiments, foliation development and associated weakening is observed after coaxial strains of only 30% or even less [e.g., *Le Hazif*, 1978; *Jordan*, 1987].

For sufficiently small ϕ_w values (<0.2), the weak phase may never become completely interconnected, but will remain locked in interstitial pockets which change their shape with strain. Under these conditions, the strength of the polyphase material depends strongly on the configuration of these interstitial spaces. The breakdown or flattening of the framework can involve brittle failure, dynamic recovery and recrystallization, grain size-sensitive creep, or a combination of these mechanisms, as occurs in feldspar in Figures 2*b* and 2*c*. The final shape and position of the domain 1 boundary curve approach that of the strength curve for a porous solid if the strength contrast between the phases is at least 10–100 [*Eudier*, 1962; *Tharp*, 1983]:

$$\sigma_{\text{rock}} = \sigma_s(1 - k\phi_w^{2/3}) \tag{1}$$

where σ_{rock} is the strength of the porous aggregate or polyphase rock, σ_s is the strength of the strong phase, and ϕ_w is the porosity or volume proportion of weak phase. The constant k is an experimentally or theoretically derived structure factor corresponding to the shape and configura-

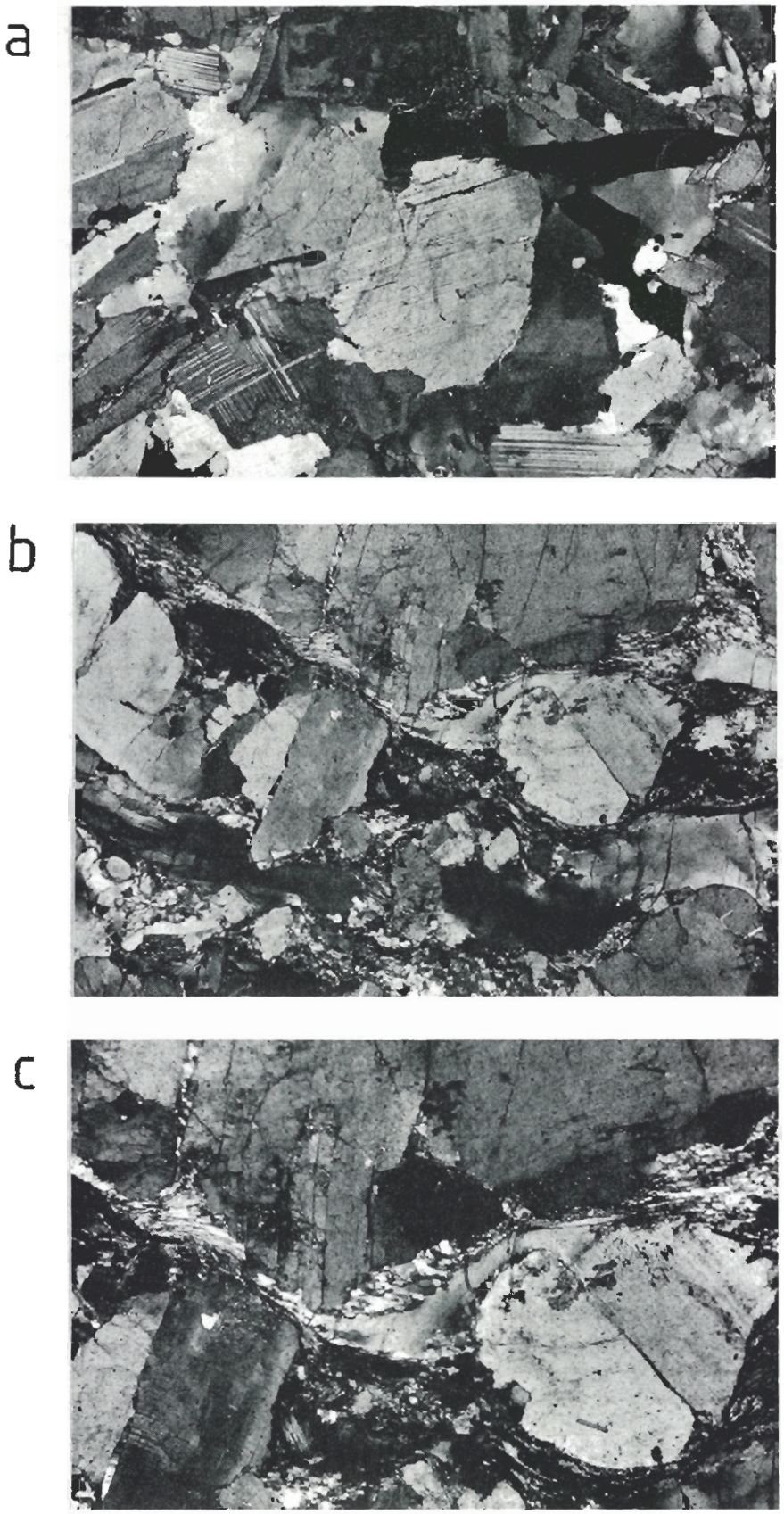

Fig. 2. Foliation development in a quartz-diorite during greenschist facies mylonitization (Pogallo Line, Southern Alps, northern Italy): (*a*) Weakly deformed diorite outside of the shear zone; feldspar grains form a load-bearing framework (5.6 × 3.8 mm). (*b*) Dioritic gneiss within the shear zone; the feldspar framework has collapsed, and interconnected strands of quartz form a foliation roughly parallel to the shear zone boundaries (5.6 × 3.8 mm). (*c*) Closeup of Figure 2*b*. Individual quartz grains are highly attenuated and partly dynamically recrystallized. Feldspar shows patchy undulose extinction, intragranular and transgranular fractures, and very limited, fine-grained dynamic recrystallization (3.6 × 2.4 mm).

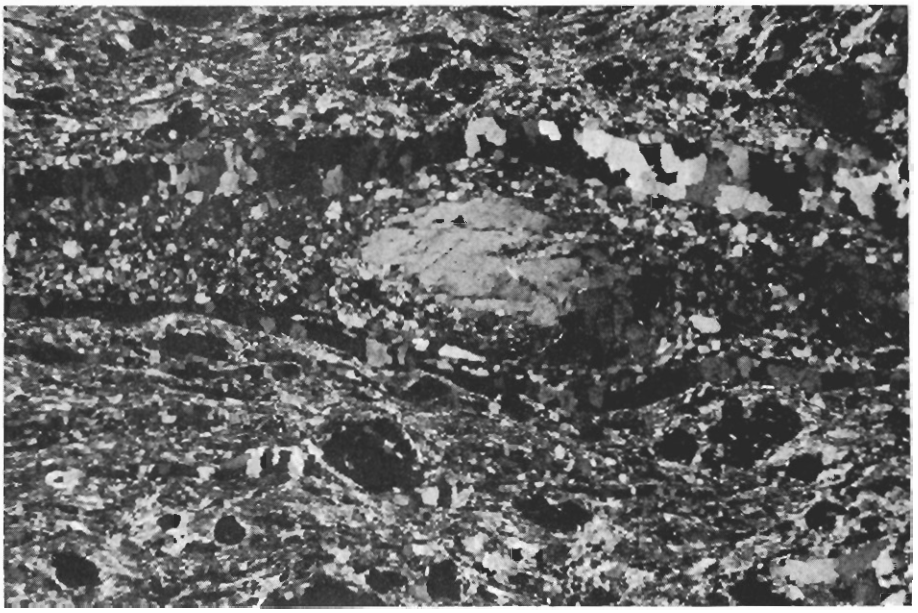

Fig. 3. Transition from a domain 3, clast-matrix microstructure to a domain 2 boudin-matrix microstructure in a mid- to upper amphibolite facies, quartzo-feldspathic mylonite (Koralps, southeastern Austria). Elongate boudins and strands of dynamically recrystallized feldspar enclose a feldspar clast and are themselves surrounded by dynamically recrystallized quartz and fine-grained biotite and white mica. Note the opaque garnet clasts in the micaceous matrix (*XZ* fabric plane, 3.9 × 2.6 mm).

tion of the interstitial space. *Griffith et al.* [1979] calculated values of k ranging from 0.98, for perfectly spherical pores with no stress concentrations in the necks (i.e., interconnected regions) of the strong phase, to 3.8 for elliptical pores with maximum stress concentrations in the neck regions. According to equation (1), increased aspect ratio of the interstitial spaces during deformation, and hence stress concentration in the neck regions connecting the grains of strong phase, results in a leftward pivot of the boundary curve in Figure 4*a* [*Jordan*, 1988]. The lower part of the domain 1 boundary curve in Figures 1 and 4 is constructed with the empirical best fit value of $k = 1.8$ for porous metals [*Ishimaru et al.*, 1971; *Tharp*, 1983]. *Jordan* [1988, Figure 5] has shown that values of $k = 1.2$ to 1.8 also fit his calcite-halite strength data at ϕ_w less than 0.3 and coaxial strains of up to 40%. At strength contrasts of 10 or less amongst the constituent minerals, the bulk and shear moduli of the weak phase are sufficiently large with respect to those of the strong phase to increase the strength of the aggregate significantly above that of a porous solid. The upper part of the domain 1 boundary curve in Figures 1 and 4 is bent upward from the predictions of equation (1) for $k = 1.8$ to reflect this expectation. At very low volume proportions of weak phase ($\phi_w < 0.1$) and for mineral strength ratios greater than one, the strength of the aggregate is predicted to exceed slightly the strength of its strongest constituent mineral as stress is concentrated into the neck regions of contiguous grains of strong phase. Accordingly, the domain 1 boundary and contours of normalized rock strength are arched convex upward at very low values of ϕ_w in Figures 1 and 4. This effect is more pronounced toward higher mineral strength ratios (see expanded diagram, top of Figure 1) but probably decreases with increasing strain as the contiguity of the strong phase increases (Figure 4*a*).

At low initial strains, the boundary between rheological

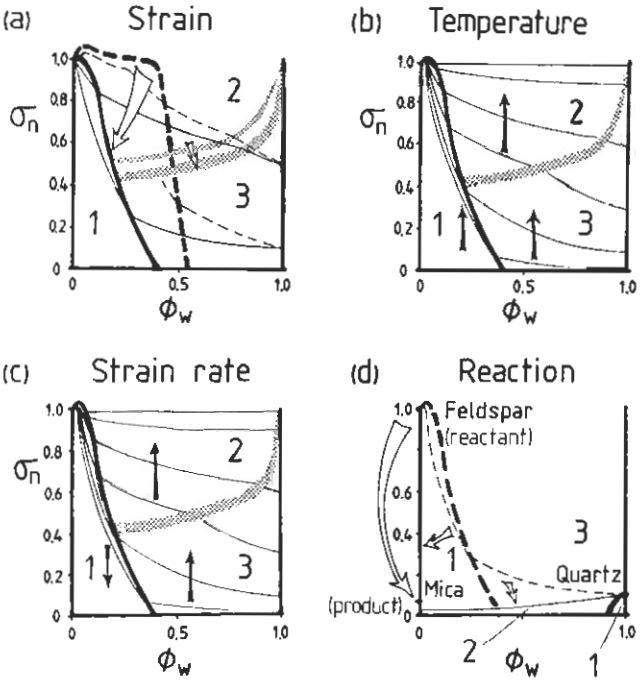

Fig. 4. Hypothetical normalized strength versus composition diagrams showing the effects of (*a*) increased strain, (*b*) increased temperature, and (*c*) increased strain rate. (*d*) The rheological consequences of the syntectonic reaction in Figure 5 (see section 3.2). Rheological domain boundaries and contours of normalized rock strength for given values of mineral strength ratio are indicated as in Figure 1. Open arrows in Figures 4*a* and 4*d* show the movement of domain boundaries and rock strength contours from positions of lower strain (dashed lines) to higher strain (solid lines). Solid arrows in Figures 4*b* and 4*c* indicate the shift in plotted position of deforming rocks with respect to the contours of normalized rock strength (see text).

domains 2 and 3 and the contours of normalized rock strength at constant mineral strength ratio in these domains migrate downward (Figure 4*a*) as the stronger phase yields at progressively higher mineral strength ratios and a foliation develops parallel to the plane of flattening. The effect of strain in domains 2 and 3 is greatest at intermediate to low values of ϕ_w because the overall reduction in stress concentration associated with foliation development is more pronounced than at higher ϕ_w (discussion in section 4.3). Due to the strain-dependent leftward pivot of the domain 1 boundary curve, the transition from framework-supported to matrix-supported behavior occurs at progressively lower values of ϕ_w (Figure 4*a*) [see also *Arzi*, 1978; *Jordan*, 1988].

Once a steady state microstructure develops in any of the domains, further strain can change the strength contrast between constituent minerals. This results in an upward or downward shift in the plotted position of a deforming rock in Figure 1 (i.e., a vertical movement relative to the contours of normalized rock strength), depending on whether the strong phase weakens or hardens with respect to the weak phase. In Figure 3, for example, progressive dynamic recrystallization of a feldspar clast is associated with a transition from domain 3 to domain 2 behavior, as inferred from the increased aspect ratio of the dynamically recrystallized feldspar aggregates in comparison to the rounded clast shape. Based on this structural evolution, feldspar is interpreted to have strain-weakened with respect to quartz.

Strain rate and temperature govern the strength contrast between constituent minerals, and so any changes in these parameters also shift the plotted position of a deforming rock in Figure 1 with respect to the contours of normalized rock strength. Strain rate and temperature are inferred to have opposite effects on the framework-supported rheology of polymineralic rocks (domain 1 in Figures 4*b* and 4*c*). Increased temperature and/or decreased strain rate reduces stress concentrations in the neck regions of the load-bearing framework and so results in an upward movement of rocks plotted in rheological domain 1 to higher values of normalized strength for any ϕ_w (i.e., k decreases in equation (1); Figure 4*b*). Conversely, the creep strength of framework-supported rocks decreases at lower temperatures and/or higher strain rates due to the increase in localized stress-concentrations (Figure 4*c*). Matrix-supported rheologies (domains 2 and 3) differ from a framework-supported rheology in that temperature and strain rate usually affect the rock strength in similar ways (compare solid arrows in Figures 4*b* and 4*c*). Increased temperature and strain rate lead to a reduction in the relative strength of most minerals, shifting the plotted position of rocks upward with respect to the contours in rheological domains 2 and 3 (Figures 4*b* and 4*c*). The temperature-dependent change in the relative strength of minerals is evidenced by the contrasting microstructural behavior of quartz and feldspar in Figures 2*c* and 3, respectively, for greenschist and amphibolite facies deformational conditions. The location of the transition point separating framework- from matrix-supported rheologies depends strongly on strain (discussion above) and on the relative temperature and strain rate dependencies of creep in the two most abundant phases that make up the rock.

Pressure effects on the creep strength of silicate rocks are likely to be minor for most lithospheric conditions because the pressure sensitivity of creep in silicates is typically much less than their temperature or strain rate sensitivities [e.g., *Paterson*, 1987]. However, low effective stresses associated with high fluid pressures can induce embrittlement and failure [e.g., *Rutter*, 1972] and so reduce bulk strength. Such strength reduction is expected to be most pronounced in domain 1 where the load-bearing strong phase is more creep resistant and hence more susceptible to embrittlement than is the weak phase at a given temperature and strain rate.

Syntectonic variations in temperature, pressure, and fluid activity can effect changes in mineral stability that alter the rheology of a deforming rock [e.g., *White and Knipe*, 1978; *Brodie and Rutter*, 1985]. Figure 5 shows two stages in the retrograde greenschist facies mylonitization of a quartzofeldspathic gneiss. Initially, dynamically recrystallized quartz is the weakest phase, with the rigid feldspar clasts undergoing incipient recrystallization and discontinuous reaction to very fine grained white mica, clinozoisite, and quartz (Figure 5*a*). With the reaction at completion (Figure 5*b*), the dynamically recrystallized quartz is boudinaged, and so the fine-grained reaction products in the matrix are inferred to be weaker. The extreme attenuation of the quartz aggregates suggests that the strength contrast between quartz and the micaceous matrix is less than an order of magnitude (see section 3). The rheological evolution inferred from the microstructures in Figure 5 is depicted schematically in Figure 4*d*. The syntectonic reaction simultaneously induces overall weakening and a switch from domain 3 clast-matrix behavior to domain 2 boudin-matrix behavior. This switch is associated with a strength inversion between the initially weaker phase (quartz), the strong solid reactant (feldspar), and the ultimately weakest solid reaction products (mica, clinozoisite). An important consequence of this evolution is that the load-bearing framework rheology is suppressed (Figure 4*d*). Therefore drastic strength drops are expected to occur in tectonites containing large volume proportions of a strong phase that is unstable and breaks down to weak, fine-grained products at the ambient conditions of deformation.

In summary, it is evident that rheology and microstructure are very closely linked in rocks. Three types of stable planar microstructure (i.e., steady state foliations as defined by *Means* [1981]) develop after only modest strains, and their formation is related to the relative strengths and volume proportions of the mineral phases in the aggregate. Variations in the physical conditions of deformation change the relative strength of these phases and so can alter the stable microstructure of a rock. The ubiquity of the microstructures shown in Figure 1 in mylonites of widely varied mineralogy and composition suggests that these microstructures reflect basic principles of dynamic equilibrium governing the flow of rheologically heterogeneous crystalline materials.

4. NATURAL AND THEORETICAL CONSTRAINTS ON POLYMINERALIC RHEOLOGY

4.1. *Stress and Strain Concentration*

Establishing the nature of the deformational processes and forces that act on the grain scale in rocks is requisite for a better theoretical characterization of polymineralic rheology. The contrasting rheological behavior of minerals can lead to complex patterns of stress and strain partitioning in a flowing aggregate, particularly in rheological domain 3.

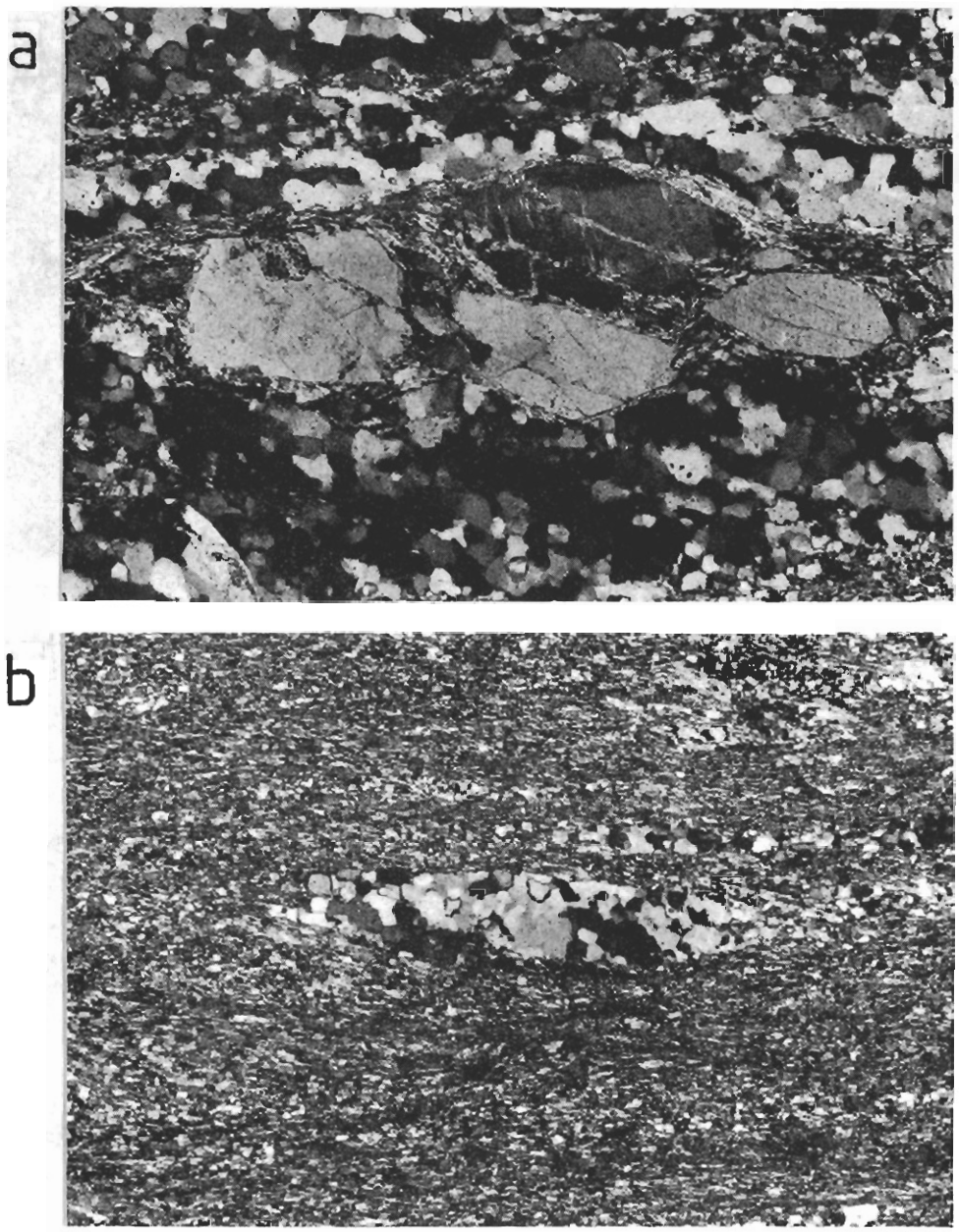

Fig. 5. Microstructural changes during a discontinuous syntectonic reaction under hydrous greenschist facies conditions, showing a transition from domain 3 to domain 2 rheology (Pogallo Line, Southern Alps, northern Italy): (*a*) Weak, dynamically recrystallized quartz matrix contains feldspar clasts undergoing incipient reaction to fine-grained white mica and clinozoisite. Note the nucleation of reaction products in fractures and clast tails (*XZ* fabric plane, 1.4 × 1 mm). (*b*) Micaceous reaction products comprise weak, fine-grained matrix that surrounds elongate boudins of fine, dynamically recrystallized quartz. The initially weaker quartz in Figure 5*a* is now slightly stronger than the micaceous reaction products (*XZ* fabric plane, 1.4 × 1 mm).

Figure 6*a* is a closeup of the domain 3 clast-matrix microstructure in a granodiorite mylonitized under greenschist facies conditions. The dynamically recrystallized quartz in the narrow areas between the feldspar clasts behaves like a liquid constricted between solid indenters. Pinched areas like these are the sites of extreme stress and strain gradients within the quartz, as evidenced by the elongation of single unrecrystallized grains (Figure 2*c*) and the significant change in dynamically recrystallized grain size (Figure 6*a*). To quantify these gradients, the grain diameter and crystallographic preferred orientation in the quartz matrix were measured in eight areas of localized microstructural steady-state (Figure 6*b*). The grain size analysis of these domains is presented graphically in Figure 6*c*. The grain diameters were measured in thin section with the line-intercept and intercept-diameter methods and then corrected for the two-dimensional truncation effect [*Exner*, 1972, pp. 32 and 33].

The crystallographic preferred orientation of the quartz grains in the eight steady state areas is strong (Figure 6*b*), indicating that dislocation creep was the dominant deformation mechanism in quartz. The varied, asymmetrical quartz *c* axis patterns suggest that shearing around the rigid feldspar clasts was highly heterogeneous and noncoaxial. A relatively high proportion of quartz *c* axes in the fine-grained, high

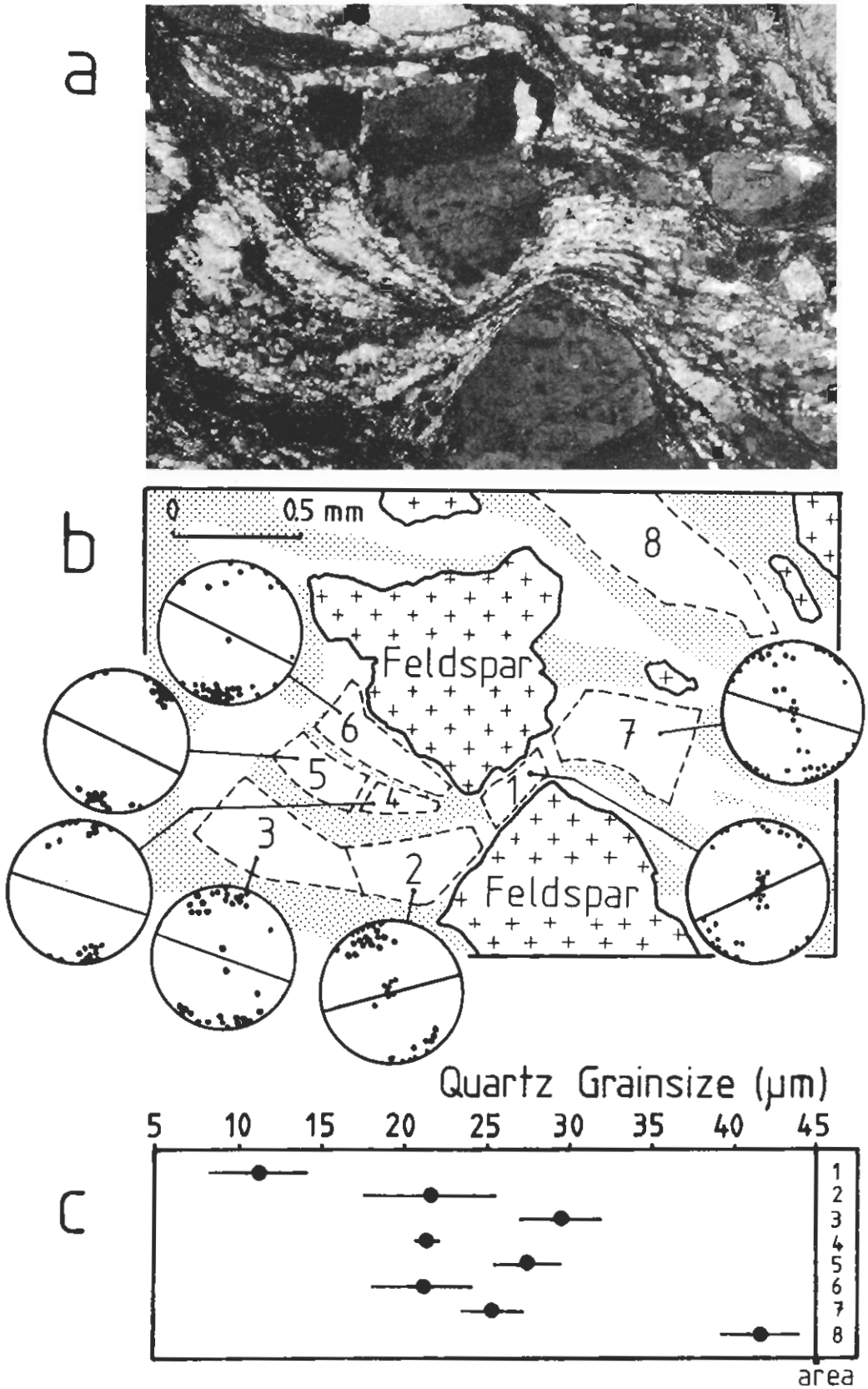

Fig. 6. Feldspar and quartz microstructures in a granodiorite mylonitized under greenschist facies conditions (Pogallo Line, Southern Alps, northern Italy): (*a*) Dynamically recrystallized quartz matrix flowing between clasts of plagioclase feldspar (*XZ* fabric plane, scale bar in Figure 6*b*). (*b*) Schematic diagram of Figure 6*a*, with microstructural areas 1–8 in quartz delimited by dashed lines. Lower hemisphere, equal-area projections indicate the distribution of *c* axes with respect to the local orientation of the foliation in areas 1–7 (see text). Finely stippled areas contain fine-grained recrystallized mica and feldspar. (*c*) Average dynamically recrystallized quartz grain size (points) with population standard deviation (bars) for the eight areas of microstructural steady state outlined in Figure 6*b*.

stress and strain regions (areas 1 and 2 in Figure 6*b*) is oriented parallel to the *Y* fabric direction in the rock. These orientations are attributed to glide on the prism {m}⟨a⟩ systems at the expense of the basal {c}⟨a⟩ and rhomb {r}⟨a⟩ and {z}⟨a⟩ systems [*Schmid and Casey*, 1986]. This accords with the widespread observation in quartzites that prism glide is activated at higher critical resolved shear stresses than basal and rhomb glide at the low homologous temperature/high strain rate conditions characteristic of greenschist facies mylonitization [e.g., *Tullis et al.*, 1973; *Schmid and Casey*, 1986]. At the same conditions of deformation, cataclasis is the dominant deformation mechanism for the feldspar (Figure 6*a*). The feldspar clasts are fragmented, show patchy undulose extinction, and only locally undergo limited dynamic recrystallization (grain size < 5 μm; see Figure 2*c*). The rounded edges of some clasts may result from the additional activity of solution transport mechanisms.

Experimental and theoretical studies in numerous metals, ceramics, and rocks indicate that dynamically recrystallized grain diameter δ is inversely proportional to the flow stress σ according to the equation [*Twiss*, 1977]

$$\sigma = L\delta^{-p} \tag{2}$$

where L and p are material constants. The p values in quartzite range from a materials best fit value of 0.68 [*Twiss*, 1977] to experimental "wet" values of 0.71 [*Mercier et al.*, 1977] and 1.11 [*Christie et al.*, 1980]. For an average p value of 0.9, the change of about 370% in the dynamically recrystallized grain size between areas 1 and 8 in Figure 6*b* corresponds to flow stress contrasts in quartz of ~300% over distances of approximately a millimeter. In order for such high mechanical and microstructural gradients to be preserved on this small scale, the rate of stress drop at the end of deformation must have far exceeded the rate at which dynamically recrystallized grain size could equilibrate with stress.

The degree of stress concentration in the quartz matrix obviously depends on clast size and spacing (Figure 7*a*). A clast size-spacing factor α is defined as the ratio of the distance between clast boundaries to the distance between the clast centers as measured along a line connecting the centers of two clasts. Alternatively, α is an expression of the ratio of average spacing to average size of the clasts. The smaller the value of α at a given clast size, the smaller the volume proportion of weak phase, ϕ_w, and the greater the stress and strain concentration between clast centers.

Figure 7*b* is a plot of dynamically recrystallized grain size in quartz versus the clast size-spacing factor for several clast-matrix pairs such as shown in Figure 6. All grain size measurements were made in the same thin section of deformed granodiorite. There are few matrix grain size measurements at α values above 0.8 (i.e., at high average clast spacing to size ratios) due to the relatively high volume proportion of feldspar clasts in this particular sample. Quartz-matrix grain size at high α values might be expected to manifest the far-field effects of several feldspar clasts rather than of just one pair of clasts. However, such far-field effects are difficult to quantify directly because the range of quartz grain sizes at high α values (δ = 28–42 μm; Figure 7*b*) is comparable to the range of grain sizes (δ = 20–50 μm) measured in quartzose layers of this rock as well as in mylonitized quartz veins from the same, regional scale shear zone [*Handy*, 1986, Figure 5.01].

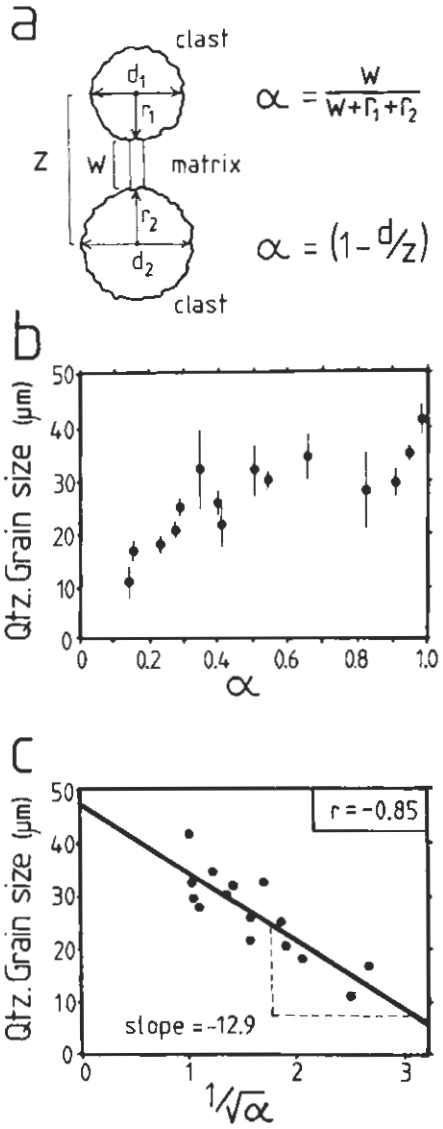

Fig. 7. Quantification of clast-matrix microstructures: (*a*) Definition of α factor in terms of the average size of clasts, d, and the spacing of clasts, z, as measured along a line connecting their centers. (*b*) Plot of dynamically recrystallized quartz grain size versus α for 15 pairs of feldspar clasts such as shown in Figure 6. Bars indicate population standard deviation. (*c*) Best fit of the quartz grain size data in Figure 7*b* to equation (3) in the text (correlation coefficient, $r = -0.85$).

Figure 7*b* shows that the plot of quartz grain diameter δ versus clast size-spacing factor α is nonlinear and is best fit by the empirical function (Figure 7c)

$$\delta = f\alpha^x + y \tag{3}$$

where the empirical constants are (for δ in μm) $f = -12.9$, $x = -0.5$, and $y = 47.3$. This relation can be used to estimate the dependence of stress concentration on clast size and spacing in quartzo-feldspathic tectonites.

Stress concentration σ_c is here defined as

$$\sigma_c = \sigma_\alpha/\sigma_{qtz} \tag{4}$$

where σ_α is the flow stress in the quartz-matrix between clasts with a specified α value and where σ_{qtz} is the flow

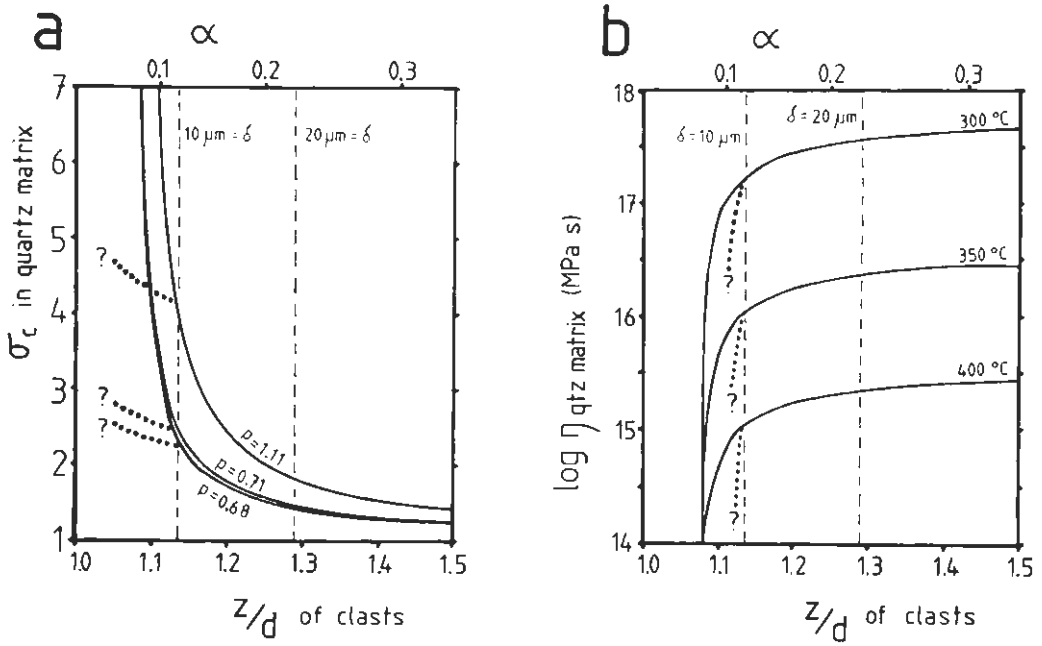

Fig. 8. (*a*) Stress concentration in the quartz matrix versus the ratio of spacing z to size d of feldspar clasts, calculated from equation (6). Piezometric stress–grain size exponents for quartz, p, taken from *Mercier et al.* [1977], *Twiss* [1977], and *Christie et al.* [1980]. Vertical dashed lines in Figures 8*a* and 8*b* indicate dynamically recrystallized grain size in the quartz matrix. (*b*) Log viscosity of quartz versus spacing to size ratio of the feldspar clasts calculated from equation (7) for a range of greenschist facies temperatures. Creep parameters for naturally hydrous quartzite taken from *Jaoul et al.* [1984]: $n = 2.4$, $Q = 163$ kJ/m, $A = 1 \times 10^{-5}$ MPa^{-n} s^{-1}. Dotted curves in Figure 8*a* and 8*b* indicate reduced stress concentration and creep viscosity, respectively, due to potential switch in deformation mechanisms in quartz at grain sizes less than ~10 μm (see text).

stress in a pure quartzite for which $\alpha = 1$ and $\delta = f + y$. Substituting equations (2) and (3) into equation (4) results in an empirical expression for stress concentration in terms of the clast size-spacing factor:

$$\sigma_c = \frac{L(f\alpha^x + y)^{-p}}{L(f + y)^{-p}} \tag{5}$$

Since $\alpha = (1 - d/z)$, equation (5) becomes

$$\sigma_c = \frac{\left[f\left(1 - \frac{d}{z}\right)^x + y\right]^{-p}}{(f + y)^{-p}} \tag{6}$$

where d and z are the average clast size and average clast spacing, respectively, and $d/z \leq 1$. The dependence of matrix viscosity η_w on clast size and clast spacing is obtained with the equation

$$\eta_w = F^{-1}[L(f\alpha^x + y)^{-p}]^{1-n} \tag{7}$$

where n is the creep exponent of the matrix material. F is usually expressed as $A \exp(-Q/RT)$, where T is the absolute temperature, Q is the activation energy of creep, A is an empirically determined constant, and R is the universal gas constant. Equations (6) and (7) are plotted in Figures 8*a* and 8*b* using the empirical values of f, x, and y for the mylonitized greenschist facies quartz-feldspar aggregates (Figure 7*c* and equation (3)) and experimental p values for quartzite in the literature (see caption of Figure 8). The experimental creep parameters in equation (7) are taken from *Jaoul et al.* [1984] for naturally hydrous quartzite (see caption of Figure 8*b*).

Figure 8*a* indicates that stress concentration in the quartz matrix is low for small clast sizes and for large spacings between clasts. Further reduction of stress concentration in the matrix is slight at clast spacing to size ratios above 1.5. Conversely, stress concentration in the matrix rises dramatically as the ratio of clast spacing to clast size decreases to 1.1. This is coupled with a drastic reduction in both stress-dependent quartz grain size and viscosity of the quartz matrix (Figure 8*b*).

The relations in Figure 8 provide a physical explanation for the microstructural observations and rheological inferences made in section 3. Grain size reduction via dynamic recrystallization enhances the ductility of the weak phase with respect to the strong phase. This allows the weak phase to accommodate a greater proportion of the strain and so to exert a disproportionately large weakening effect on the bulk strength of the aggregate (asymmetrical contours in Figure 1). The reduction of stress concentration associated with cataclasis of the strong phase is partly responsible for the strain-dependent decrease of bulk strength in domain 3. As will be shown in section 4.3, the strain-dependent development of a foliation involves an increase in the average spacing of the strong phase particles and so also contributes to an overall reduction in stress concentration.

The dramatic rise in stress concentration at low clast spacing to size ratios (Figure 8*a*) suggests that hydrodynamic lubrication forces in the dynamically recrystallized quartz matrix govern clast interactions and exert a major influence

on the microstructure. Lubrication theory predicts that infinite forces are required to push surfaces together at finite velocity [*Frankel and Acrivos*, 1967]. However, the fact that feldspar clasts are often observed to be in mutal contact indicates that lubrication theory does not apply at very low z/d ratios. In nature, several mechanical factors place upper limits on stress concentration in the weak matrix. High localized stresses can exceed the fracture strength of one or more of the constituent minerals and so lead to cataclasis and an associated reduction in stress concentration. Alternatively, the stress-dependent dynamically recrystallized grain size in the matrix becomes sufficiently small to induce a change in creep mechanism from dislocation creep to grain size–sensitive diffusion creep. Such a mechanism switch is associated with large reductions in matrix viscosity for a given temperature and strain rate [e.g., *Schmid*, 1982]. For quartz creeping at greenschist facies conditions and geological strain rates, this switch occurs at grain sizes of ~10 μm or less (Figures 8*a* and 8*b* [*Behrmann*, 1985]) At conditions favoring low strength contrasts amongst all phases (domain 2 rheology in Figure 1), stress concentration in the matrix can induce yielding and crystal plastic flow in the strong, hitherto rheologically passive phases. The feedback effect this has on stress concentration in the matrix is indicated schematically with dotted lines in Figures 8*a* and 8*b*. Stress-induced changes in the deformation mechanism of the weak phase or yielding of the strong phase both result in a reduction in stress concentration and an overall decrease in rock strength.

4.2. *Partitioning of Strain Energy*

The examples in section 3 show that strain partitioning amongst the mineral phases in a deforming rock is clearly tied to variations in the microstructure of that rock, as well as to the physical conditions of the deformation. In this section, a hypothesis is advanced which relates composition-dependent stress- and strain rate partitioning to the bulk strength of a deforming aggregate. This facilitates the estimation of polymineralic rock strength from a combination of mechanical and microstructural information on its constituent minerals.

At the heart of this hypothesis is the notion that deformational work and work rate done on a rock are additive. In other words, the strain energy expended on an aggregate is equal to the sum of the strain energy expended on every part of that aggregate, regardless of rock composition. For an aggregate in which all constituents undergo steady state flow, the additive strain energy condition is expressed as

$$\sum_{i=1}^{N} \sigma_i \dot{\varepsilon}_i = \sigma_{\text{rock}} \dot{\varepsilon}_{\text{rock}} \tag{8}$$

where σ_i and ε_i are the stress and strain rate of the ith constituent phase in a rock of strength σ_{rock} deforming at strain rate $\dot{\varepsilon}_{\text{rock}}$. For constant volume creep in which strain compatibility is maintained amongst the constituent phases in the aggregate, strain, and hence also strain rate must be additive, irrespective of the microstructure of the aggregate:

$$\sum_{i=1}^{N} \phi_i \dot{\varepsilon}_i = \dot{\varepsilon}_{\text{rock}} \tag{9}$$

where ϕ_i is the volume proportion of the ith phase in the aggregate. A formal theoretical treatment of stress partitioning in polyphase aggregates lies beyond the scope of this paper, but the empirical relation in equation (6) can be used to constrain the dependence of stress partitioning on the size and distribution of phases in a quartzo-feldspathic rock. With the energetic and compositional constraints in equations (8) and (9), one can estimate the rock strength from the stresses and strains in i-1 minerals in a rock. From equation (9), it follows that the unknown strain rate of any phase or phases in a rock can be determined from knowledge of the bulk strain rate and the measured strain rate of the remaining phase or phases. For a simple bimineralic rock containing minerals i and j, this is expressed as

$$\dot{\varepsilon}_j = \frac{\dot{\varepsilon}_{\text{rock}} - \phi_i \dot{\varepsilon}_i}{1 - \phi_i} \tag{10}$$

The strain rate of the phases can be expressed in terms of flow stress, provided that a steady state constitutive equation is available [*Weertman*, 1968]:

$$\dot{\varepsilon} = F\sigma^n \tag{11}$$

where n is the stress exponent and F has been defined in equation (7).

Solving equation (8) for bulk strength σ_{rock} and substituting equations (10) and (11) yields a relation which expresses rock strength in terms of the bulk strain rate, the volume proportion of phases in the rock, the creep parameters of those phases, and either the stress or the strain rate in one of the phases:

$$\sigma_{\text{rock}} = \frac{\dot{\varepsilon}_i[\exp n_i^{-1} + F_i^{-1}\dot{\varepsilon}_i] + F_j\sigma_j^{n_j+1}}{\dot{\varepsilon}_{\text{rock}}} \tag{12}$$

and

$$\dot{\varepsilon}_i = \frac{\dot{\varepsilon}_{\text{rock}} - \phi_j F_j \sigma_j^{n_j}}{1 - \phi_j}$$

This equation is relevant for the case in which the stresses and volume proportions of all phases are obtained from piezometry and point count analysis of thin sections of naturally deformed rock. Alternatively, if the strain rates of all phases are determined from direct observation of the evolving microstructure in experimentally deforming rock analogues,

$$\sigma_{\text{rock}} = \frac{\dot{\varepsilon}_i[\dot{\varepsilon}_i F_i^{-1} + \exp n_i^{-1}] + \dot{\varepsilon}_j[\dot{\varepsilon}_j F_j^{-1} + \exp n_j^{-1}]}{\dot{\varepsilon}_{\text{rock}}} \tag{13}$$

In this equation, composition is expressed implicitly through the different strain rates measured for the constituent phases. Synkinematic microscopy of experimentally deforming rock analogues is a promising way of testing the validity of the strain energy partitioning hypothesis for polyphase aggregates.

Equations (12) and (13) are general expressions for domain 2 polymineralic rheology, in which both of the constituent phases in a bimineralic rock are rheologically active. A basic assumption made is that all of the rheologically active phases in the deforming aggregate undergo steady state flow. Microstructural evidence of work hardening and elastic/

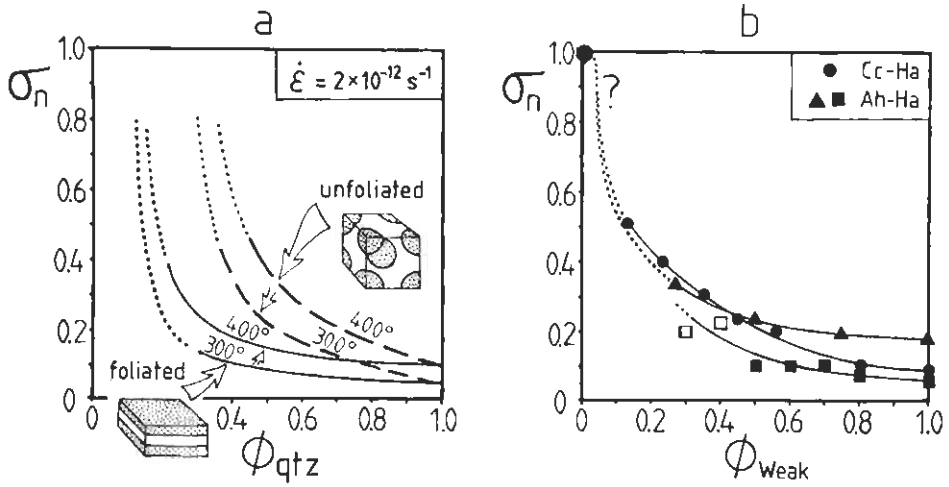

Fig. 9. Creep strength versus composition relations: (*a*) Normalized rock strength at constant mineral strength contrast (10 : 1 to 20 : 1) calculated from equation (15) for domain 3 rheology in a quartz-feldspar rock at greenschist facies conditions (T = 300°–400°C). Dashed lines indicate rock strength for an idealized, body-centered cubic configuration of feldspar clasts at low strains (equation (16)). Solid lines represent rock strength for a quartzo-feldspathic aggregate with a perfectly planar foliation parallel to the shearing plane (see text). Dots show those portions of the curves which lie in rheological domains 1 or 2 and are therefore not strictly valid. Feldspar creep parameters [*Shelton and Tullis*, 1981]: n = 3.9, Q = 234 kJ/m; A = 2.4 × 10^{-6} MPa^{-n} s^{-1}. Quartz creep parameters as in Figure 8*b*. (*b*) Normalized rock strength at constant mineral strength contrast (5 : 1 to 20 : 1) for experimentally deformed aggregates. Circles, calcite-halite aggregates of *Jordan* [1987] at ε = 35%, T = 200°C, P = 150 MPa, $\dot{\varepsilon}$ = 10^{-4} s^{-1}; triangles, anhydrite-halite aggregates of *Price* [1982] at ε = 10%, T = 200°C, P = 200 *MPa*, $\dot{\varepsilon}$ = 10^{-4} *s*$^{-1}$; solid squares, anhydrite-halite aggregates of *Ross et al.* [1987] at ε = 3.5%, T = 300°C, P = 200 MPa, axial displacement rate of 5 × 10^{-6} cm/s; open squares, for steady state behavior at ε = 5%. Solid portions of curves are valid for clast-matrix rheology, dotted portions for compositional ranges over which strength data are unavailable or for which a framework-supported rheology predominates.

frictional deformation in mylonites is largely restricted to the rheologically passive phase(s) that characterize domain 3 polymineralic rheology (see Figure 2). Although non–steady state behavior of the strong phase could be incorporated into the hypothesis above, its contribution to the total strain energy is probably small compared with the strain energy of plastic creep in the weakest phase(s).

4.3. *Applications to Foliation Development in Rocks*

The microstructures analyzed in section 4.1 can be used together with the concepts developed in the last section to predict domain 3 clast-matrix rheology in a quartz-feldspar tectonite. For domain 3 rheology, the internal deformation of the strong phases is very small (feldspar clasts in Figures 2 and 6), so their rheological effect is solely to concentrate stress and strain-rate into the quartz matrix. Thus the strength of the aggregate depends on the bulk strain rate, the strength and strain rate of the quartz matrix, and on the distribution and volume proportion of feldspar. Simplification of equation (12) leads to a basic expression for the normalized strength of a bimineralic aggregate with clast-matrix rheology:

$$\sigma_n = \frac{\sigma_{\text{rock}}}{\sigma_s} = \frac{\sigma_w \dot{\varepsilon}_w}{\sigma_s \dot{\varepsilon}_{\text{rock}}} \tag{14}$$

where all of the variables and subscripts have been defined above. After substitution of equations (2), (3), and (11) into equation (14), the full expression for normalized rock strength is

$$\sigma_n = \frac{F_w[L(f\alpha^x + y)^{-p}]^{n_s - 1}}{\dot{\varepsilon}_{\text{rock}} \exp\left[n_s^{-1} \ln \dot{\varepsilon}_{\text{rock}} F_s^{-1}\right]} \tag{15}$$

Equation (15) is plotted in Figure 9*a* for an estimated bulk strain rate of 2 × 10^{-12} s^{-1} and mid to upper greenschist facies temperatures (300°–400°C) in the quartzo-feldspathic mylonite shown in Figure 6*a*. The volume proportion of quartz in the aggregate, ϕ_{qtz}, is equated with α values from 0 to 1. Experimental creep parameters for the constituent phases are taken from *Shelton and Tullis* [1981] for feldspar (Hale albite rock) and from *Jaoul et al.* [1984] for quartzite (naturally hydrous Heavitree quartzite). There is significant variation amongst experimentally determined creep parameters in each material [e.g., *Kirby and Kronenberg*, 1987, Table 3], and the experimental errors propagate when the creep laws are extrapolated to natural strain rates [*Paterson*, 1987]. However, this does not alter the qualitative conclusions drawn below.

Two pairs of curves of normalized rock strength are depicted in Figure 9*a*. The lower of the two curves at a given temperature and mineral strength contrast describes the strength of an aggregate with a perfectly planar distribution of strong and weak phases after high-strain deformation. These normalized strength curves are obtained via direct substitution of the ϕ_w values for the clast spacing to size factor α in equation (15). There are no localized stress concentrations in this deforming aggregate, because the feldspar is contained within perfectly planar foliational layers parallel to the shearing plane. The upper of the two curves at a given temperature and mineral strength contrast

in Figure 9*a* represents the normalized rock strength for aggregates with a body-centered cubic configuration of feldspar clasts. This configuration corresponds to an idealized, zero strain arrangement of feldspar clasts in which clast spacing is minimized and stress concentration in the quartz matrix is maximized. For a body-centered cubic configuration of clasts, the expression for the α factor in terms of ϕ_w that is substituted into equation (15) is

$$\alpha = 1 - \left[\frac{3}{\pi}(1 - \phi_w)\right]^{1/3} \tag{16}$$

The shape, slope, and relative position of the curves of normalized rock strength in Figure 9*a* accord with the inferences made in section 3.2 regarding the disproportionately strong rheological influence of the weak phase and the strain dependence of rock strength in rheological domain 3. The lower bulk strength associated with the presence of a foliation can be attributed solely to the increase in average spacing between feldspar clasts if the average clast size is assumed to remain constant (recall equation (6) and Figure 8*a*). However, in naturally deformed rocks this increased spacing effect probably operates together with grainsize reduction of both clasts and matrix to reduce the bulk strength (see Figures 2*a* and 2*b*). Both pairs of strength curves in Figure 9*a* are only valid for end-member geometrical distributions of clasts in a two-phase aggregate and therefore are expected to bracket the normalized strength composition curves for naturally and experimentally deformed bimineralic aggregates at similar mineral strength contrasts. Comparison of Figures 9*a* and 9*b* suggests that this is indeed the case. The experimentally deformed bimineralic aggregates whose normalized strength curves appear in Figure 9*b* all display a strong foliation parallel to the plane of finite extension [*Price*, 1982; *Jordan*, 1987, Figure 1; *Ross et al.*, 1987, Figures 4 and 6]. Observed in detail, the clasts comprising the foliational layers are broken, often irregularly shaped [Jordan, 1987, Figure 2] and display the same general shape and distribution characteristics as the feldspar clasts in Figures 2*b*, 2*c*, and 6. The stress concentrations introduced by such geometrical irregularities within foliated layers increase the average strength of an aggregate (for a given composition) to levels above those predicted for an ideal planar foliation.

Foliation development in domains 2 and 3 is therefore seen as a mechanism of simultaneously reducing the size of stronger, rheologically less active or passive phases and redistributing these phases so that their average spacing is increased. This results in an increase in the overall contiguity of the weak matrix phase (i.e., an increase in the fraction of surface area of the weak phase that is shared with grains of that weak phase). These effects decrease the stress concentration in the weak matrix and hence reduce the amount of deformational energy expended on the aggregate for a given increment of strain. Consequently, foliation decreases the strength of the aggregate at given composition. Figure 9*a* shows that these effects are more pronounced toward low volume proportions of the weak phase, where strain compatibility in the aggregate becomes more difficult to maintain (recall sections 3.1 and 3.2)

Numerical simulation of Newtonian suspensions in simple shear [*Brady and Bossis*, 1985] indicates that the increased nonlinearity of strength with increased volume proportion of strong phase is related to "clustering" of the strong particles, a direct result of the hydrodynamic lubrication forces that prevent the strong particles in suspension from touching [*Frankel and Acrivos*, 1967]. Clustering increases nonlinearly at high volume proportions of the strong phase. It is suggested here that the clustering of strong particles observed in such suspension modelling is related to mechanically induced foliation development in experimentally and naturally deformed rocks with matrix-controlled rheologies. Aggregates or clusters of close, strong grains act as large, single-layer particles because lubrication forces transmit far-field forces between clustered grains. The process of clustering may be a self-propagating instability, such that hydrodynamic forces segregate clustered grains into ever larger layered aggregates that align parallel with the shearing plane. A steady state foliation is attained when the forces repelling clustered aggregates are in dynamic equilibrium with the dispersive forces acting between grains within the clusters. The magnitude of these forces is nonlinearly proportional to the bulk strain rate.

Future work along these lines that is relevant to rock mechanics would also account for the strongly non-Newtonian creep of most rocks as well as for the compatibility problems which arise from the highly irregular shape of clast-forming minerals at strength contrasts of 10 or greater. Finally, better characterization of the forces that act within the viscous matrix material should clarify why lubrication forces are modified or breakdown at the small clast spacings that typify dense suspensions in some rocks.

5. IMPLICATIONS FOR LITHOSPHERIC RHEOLOGY

The solid-state rheology of rocks depends primarily on the relative proportions of weak and strong minerals, the shape and distribution of these minerals, and the physical conditions of deformation. The three types of rheological behavior outlined in this paper can be related to specific structural and compositional settings in the lithosphere. In many rocks, composition and physical conditions are such that one mineral forms an interconnected matrix which is sufficiently weak to govern the bulk flow. This is widely observed in quartz-rich rocks (i.e., granites, granodiorites) under metamorphic conditions ranging from greenschist to granulite facies (250°–800°C). Salts, hydrous sulphates, and carbonates have significantly lower strengths than do silicates at temperatures below ~300°C [*Carter*, 1976; *Schmid*, 1982] so that the rheology of these rocks is matrix-controlled, even at comparitively shallow levels in the crust for the usual range of geothermal gradients. Silicate rocks in which two or more rheologically active minerals control the rheology are most likely found in the lower crust or in narrow ultramylonitic fault zones. These settings provide the high temperatures and/or small syntectonic grain sizes and high strain rates that are necessary to reduce the strength contrast amongst even the most flow-resistant minerals. Although highly deformed rocks with this type of rheology comprise only a small volume proportion of the lithosphere, they probably govern the long-term, high-strain rheology of the lithosphere due to their low viscosities. Rheology determined by a load-bearing framework of strong phases is generally restricted to some very basic lower crustal/upper mantle rocks (e.g., diorites, pyroxenites) that comprise a minor part of the lithosphere. Such rocks are particularly susceptible to cataclasis and/or

to local reaction-enhanced switches to matrix-controlled rheologies if they are emplaced into crustal levels where their mineral assemblages become unstable and where the ambient conditions of deformation increase the rock strength and the mineral strength contrasts.

The principles of strain energy partitioning in polymineralic tectonites can also be applied to the large-scale rheology of a compositionally or mechanically heterogeneous lithospheric section. Accordingly, stress and strain rate are coupled on a regional scale so that stronger rocks will deform more slowly than do weaker rocks. This suggests that strength contrasts between different lithorheological domains in the lithosphere are less pronounced than is commonly predicted from the extrapolation of monomineralic creep laws to a constant regional strain rate. More sophisticated rheological modelling of the lithosphere will account for the effects of strain and evolving pressure-temperature conditions on the rheology of polymineralic rocks.

Acknowledgments. The ideas in this paper were first presented in an informal seminar at Imperial College, London. Their subsequent evolution owes much to discussions with numerous colleagues, particularly Steve Covey-Crump, Peter Jordan, Renée Panozzo, Adrian Pfiffner, Dave Prior, and Holger Stuenitz. Steve Kirby and Jan Tullis are thanked especially for their constructive reviews. A third, anonymous reviewer offered advice on shortening the earlier version of this paper. The support of the Swiss National Science Foundation in the form of a postdoctoral grant and project 2971-0.88 is acknowledged.

REFERENCES

Arzi, A. A., Critical phenomena in the rheology of partially melted rocks, *Tectonophysics*, *44*, 173–184, 1978.

Behrmann, J. H., Crystal plasticity and superplasticity in quartzite: A natural example, *Tectonophysics*, *115*, 101–129, 1985.

Bilby, B. A., J. D. Eshelby, and A. K. Kundu, The change of shape of a viscous ellipsoidal region embedded in a slowly deforming matrix having a different viscosity, *Tectonophysics*, *28*, 265–274, 1975.

Bouillot, J. L., C. Camoin, M. Belzons, R. Blanc, and E. Guyon, Experiments on 2-D suspensions, *Adv. Colloid Interface Sci.*, *17*, 299–305, 1982.

Brace, W. F., and D. L. Kohlstedt, Limits on lithosphere stress imposed by laboratory experiments, *J. Geophys. Res.*, *85*, 6248–6252, 1980.

Brady, J. F., and G. Bossis, The rheology of concentrated suspensions of spheres in simple shear flow by numerical simulation, *J. Fluid Mech.*, *155*, 105–129, 1985.

Brodie, K., and E. H. Rutter, On the relationship between deformation and metamorphism with special reference to the behaviour of basic rocks, in *Kinetics, Textures and Deformation, Adv. Phys. Geochem.*, vol. 4, edited by A. B. Thompson and D. Rubie, pp. 138–179, Springer-Verlag, New York, 1985.

Carter, N. L., Steady-state flow of rocks, *Rev. Geophys.*, *14*(3), 301–360, 1976.

Carter, N. L., and M. C. Tsenn, Flow properties of continental lithosphere, *Tectonophysics*, *136*, 27–63, 1987.

Carter, N. L., D. A. Anderson, F. D. Hansen, and R. L. Kranz, Creep and creep rupture of granitic rocks, in *Mechanical Behaviour of Rocks, Geophys. Monogr. Ser.*, vol. 24, edited by N. L. Carter, M. Friedman, J. M. Logan, and D. W. Stearns, pp. 61–82, AGU, Washington, D. C., 1981.

Chen, I. W., and A. S. Argon, Steady state power-law creep in heterogeneous alloys with coarse microstructures, *Acta Metall.*, *27*, 785–791, 1978.

Christie, J. M., Ord, A. and P. S. Koch, Relationship Between Recrystallized Grainsize and Flow Stress in Experimentally Deformed Quartzite (abstract), *Eos Trans. AGU*, *61*(17), 377, 1980.

Einstein, A., Eine neue Bestimmung der Moleküldimensionen, *Ann. Phys.*, *19*, 289–306, 1906.

Einstein, A., Berichtigung zu meiner Arbeit: "Eine neue Bestimmung der Moleküldimensionen", *Ann. Phys.*, *34*, 591–592, 1911.

Eudier, M., The mechanical properties of sintered low-alloy steels, *Powder Metall.*, *5*, 278–290, 1962.

Exner, H. E., Analysis of grain- and particle-size distributions in metallic materials, *Int. Metall. Rev.*, *17*, 25–42, 1972.

Frankel, N. A., and A. Acrivos, On the viscosity of a concentrated suspension of solid spheres, *Chem. Eng. Sci.*, *22*, 847–853, 1967.

Gadala-Maria, F. A., and A. Acrivos, Shear-induced structure in a concentrated suspension of solid spheres, *J. Rheol.*, *24*, 799–814, 1980.

Gay, N. C., Pure shear and simple shear deformation of inhomogeneous viscous fluids, I, Theory, *Tectonophysics*, *5*(3), 211–234, 1968.

Griffith, T. J., R. Davies, and M. B. Basset, Analytical study of effects of pore geometry on tensile strength of porous materials, *Powder Metall.*, *22*, 119–123, 1979.

Handy, M. R., The structure and rheological evolution of the Pogallo fault zone: A deep crustal dislocation in the southern Alps of northwestern Italy, Ph.D. thesis, 327 pp., Univ. Basel, Switzerland, June 1986.

Hill, R., Continuum micro-mechanics of elastoplastic polycrystals, *J. Mech. Phys. Solids*, *13*, 89–101, 1965.

Horowitz, F. G., T. E. Tullis, A. Kronenberg, J. Tullis, and A. Neddleman, Finite element model of polyphase flow (abstract), *Eos Trans. AGU*, *62*(17), 396–397, 1981.

Hutchinson, J. W., Bounds and self-consistent estimates for creep of polycrystalline materials, *Proc. R. Soc. London, Ser. A*, *348*, 101–127, 1976.

Ishimaru, Y., Y. Saito, and Y. Nishino, On the properties of stainless steel P/M ferous alloys, *Mod. Dev. Powder Metall.*, *4*, 441–450, 1971.

Jaoul, O., J. Tullis, and A. Kronenberg, The effect of varying water content on the behaviour of Heavitree quartzite, *J. Geophys. Res.*, *89*, 4298–4312, 1984.

Jordan, P., The deformational behaviour of bimineralic limestone-halite aggregates, *Tectonophysics*, *135*, 185–197, 1987.

Jordan, P., The rheology of polymineralic rocks—An approach, *Geol. Rundsch.*, *77*(1), 285–294, 1988.

Kirby, S. H., Tectonic stresses in the lithosphere: Constraints provided by the experimental deformation of rocks, *J. Geophys. Res.*, *85*, 6353–6363, 1980.

Kirby, S. H., and A. K. Kronenberg, Rheology of the lithosphere: Selected topics, *Rev. Geophys.*, *25*, 1219–1244, 1987.

Kronenberg, A., and G. Shelton, Deformation microstructures in experimentally deformed Maryland diabase, *J. Struct. Geol.*, *2*(3), 341–353, 1980.

Le Hazif, R., Deformation plastique du system biphase Fe-Ag, *Acta Metall.*, *36*, 247–257, 1978.

Means, W. D., The concept of steady-state foliation, *Tectonophysics*, *78*, 179–199, 1981.

Mercier, J. C., D. A. Anderson, and N. L. Carter, Stress in the lithosphere: Inferences from steady-state flow of rocks, *Pure Appl. Geophys.*, *115*, 199–226, 1977.

Paterson, M. S., Problems in the extrapolation of laboratory rheological data, *Tectonophysics*, *133*, 33–43, 1987.

Pätzold, R., Die Abhängigkeit des Fliessverhaltens konzentrierter Kugelsuspensionen von der Strömungsform: Ein Vergleich der Viskosität in Scher- und Dehnströmungen, *Rheol. Acta*, *11*, 322–344, 1980.

Price, R. H., Effects of anhydrite and pressure on the mechanical behavior of synthetic Rocksalt, *Geophys. Res. Lett.*, *9*(9), 1029–1032, 1982.

Roscoe, R., The viscosity of suspensions of rigid spheres, *Br. J. Appl. Phys.*, *3*, 267–269, 1952.

Ross, J. V., S. J. Bauer, and F. D. Hansen, Textural evolution of synthetic anhydrite-halite mylonites, *Tectonophysics*, *140*, 307–326, 1987.

Rutter, E. H., The influence of interstitial water on the rheological behaviour of calcite rocks, *Tectonophysics*, *14*, 13–33, 1972.

Ryerson, F. J., H. C. Weed, and A. J. Piwinski, Rheology of subsolidus magmas, 1, Picritic compositions, *J. Geophys. Res.*, *93*, 3421–3436, 1988.

Schmid, S. M., Microfabric studies as indicators of deformation

mechanisms and flow laws operative in mountain building, in *Mountain Building Processes*, edited by K. J. Hsü, pp. 95–110, Academic, San Diego, Calif., 1982.

Schmid, S. M., and M. Casey, Complete fabric analysis of some commonly observed quartz c-axis patterns, in *Mineral and Rock Deformation: Laboratory Studies, Geophys. Monogr. Ser.*, vol. 36, edited by B. E. Hobbs and H. C. Heard, pp. 236–286, AGU, Washington, D. C., 1986.

Scott, A., Polyphase flow in rocks: Preliminary investigation into the "tail" development around a recrystallizing porphyroclast in a shearing matrix using a computational technique, M.Sc. thesis, Imp. Coll., London, 1987.

Shelton, G., and J. Tullis, Experimental Flow Laws for Crustal Rocks (abstract), *Eos Trans. AGU*, *62*(17), 396, 1981.

Tharp, T. M., Analogies between the high-temperature deformation of polyphase rocks and the mechanical behaviour of porous powder metal, *Tectonophysics*, *96*, T1-T11, 1983.

Tullis, J., J. Christie, and D. Griggs, Microstructures and Preferred Orientations of Experimentally Deformed Quartzites, *Geol. Soc. Am. Bull.*, *84*(1), 297–314, 1973.

Twiss, R. J., Theory and applicability of a recrystallized grainsize paleopiezometer, *Pure Appl. Geophys.*, *115*, 227–244, 1977.

Van der Molen, I., and M. S. Paterson, Experimental deformation of a partially melted granite, *Contrib. Mineral. Petrol.*, *70*, 299–318, 1979.

Weertman, J., Dislocation climb theory of steady-state creep, *Trans. Am. Soc. Metals*, *61*, 681–694, 1968.

White, S., The effects of strain on the microstructures, fabrics and deformation mechanisms in quartzites, *Philos. Trans. R. Soc. London, Ser. A*, *283*, 69–86, 1976.

White, S. H., and R. J. Knipe, Transformation- and reaction-enhanced ductility in rocks, *J. Geol. Soc. London*, *135*, 513–516, 1978.

White, S. H., S. E. Burrows, J. Carreras, N. D. Shaw, and F. J. Humphreys, On mylonites in ductile shear zones, *J. Struct. Geol.*, *1*(2), 175–187, 1980.

M. R. Handy, Geologisches Institut, Universität Bern, Baltzerstrasse 1, 3012 Bern, Switzerland.

(Received January 26, 1988;
revised September 14, 1989;
accepted December 28, 1989.)